ELSEVIER

Wear 236 (1999) 315–327

WEAR

www.elsevier.com/locate/wear

The friction and wear of Kevlar 49 sliding against aluminium at low velocity under high contact pressures

I.F. Brown *, C.J. Burgoyne

Engineering Department, University of Cambridge, Trumpington Street, Cambridge CB2 1PZ, UK

Received 12 May 1999; received in revised form 23 July 1999; accepted 29 July 1999

Abstract

The friction and wear behaviour of Kevlar 49 sliding against aluminium under large contact pressures at low sliding velocities was examined. Kevlar 49 on aluminium friction is measured using yarns on capstans, and compared with literature results for Kevlar 49 on itself. A modified version of Howell's equation is presented in terms of stresses, $\tau = a\sigma^{\beta}$, to allow finite element modelling of rope terminations. For Kevlar 49-on-aluminium this takes the form $\tau_s = 0.099\sigma^{0.91}$ and $\tau_d = 0.095\sigma^{0.91}$. Kevlar 49-on-Kevlar 49 friction is not so critical in the mechanics of the terminations as it is greater ($\mu \rightarrow 0.22$ at high pressures). Medium scale tests using yarns of 1000 filaments around capstan discs of radii 10–80 mm were performed; these are compared with large scale tests on 6 and 60 tonne rope terminations. In both situations the wear rate is calculated from the number of cycles to failure for a given severity regime. The wear rate is found to be directly proportional to the normal load for five orders of magnitude of load (6–40000 N), so Kevlar 49-on-aluminium abrasion can be expressed in terms of the Archard wear equation. The dimensional wear coefficient is found to depend strongly on the amplitude of slip present, rising from 1.0×10^{-5} mm^3(Nm)$^{-1}$ at 40 μm to 1.0×10^{-2} mm^3(Nm)$^{-1}$ at 3 mm peak to peak displacement.

Keywords: Kevlar; Aramid; Archard; Howell

1. Introduction

The purpose of these tests was to investigate the mechanics within a spike and barrel parallel-lay rope termination as shown in Fig. 1. Ropes made from parallel aramid yarns have been used for many years due to their light weight, good electrical properties and utilisation of the material's stiffness. The standard termination for these parallel-lay (Parafil) ropes is a ''spike-and-barrel'' developed by the rope manufacturer. The terminations perform very well under static loading, in long ropes failure normally occurs away from the terminations. However, the terminations may fail due to abrasion of the rope near the nose of the spike when exposed to high cyclic stresses.

Spike-and-barrel terminations for parallel-lay ropes are much more complex than they first appear. The functioning of the termination is heavily influenced by geometry, the material properties of both the termination and fibre, and the frictional properties. Any alteration to one of these factors alters the behaviour of the whole termination. Over their 25-year history, Parafil terminations have evolved into a sophisticated design. To improve on their performance, this study has looked inside the terminations and exposed hitherto unknown mechanisms and processes of slip and wear [1].

No straightforward analysis is possible because the simplifying assumptions mask the subtleties of the design. The use of a modified Howell's equation for friction, $\tau = a\sigma^{\beta}$, is proposed here to model the friction between polymeric materials. This re-expression in terms of stress enables its use in a finite element analysis. Experiments on Kevlar 49 yarns over aluminium capstans were performed to determine the stick and slip coefficients of friction.

Kevlar 49-on-aluminium abrasion tests were performed and the Archard wear equation was applied by calculating the contact pressure, amplitude of slip and thickness to be abraded. This equation is also applied to literature data for 6 and 60 tonne Parafil terminations under various cyclic

* Corresponding author. Hyder Special Structures, 29 Bressenden Place, London SW1E 5DZ, UK. Tel.: +44-171-316-6033; fax: +44-171-316-6215; E-mail: ian@fitzroy.com

0043-1648/99/$ - see front matter
PII: S0043-1648(99)00293-8

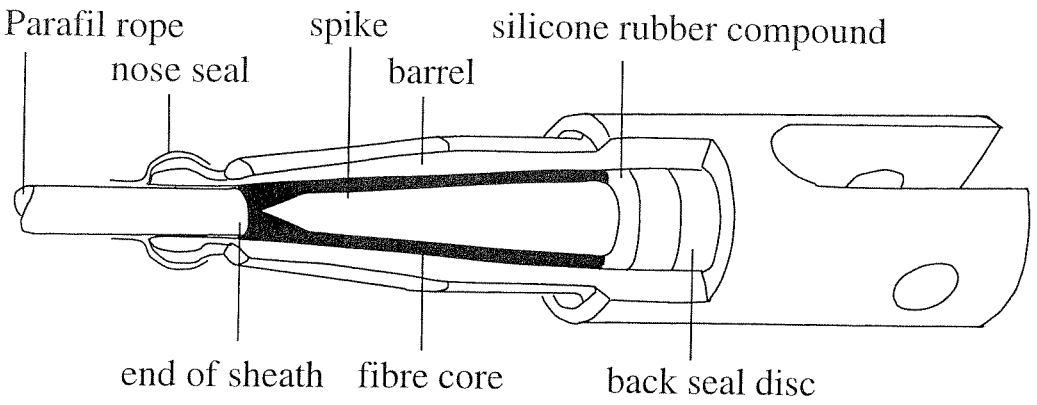

Fig. 1. Spike and barrel Parafil termination.

regimes. These two very different scales of tests show very good agreement.

2. Friction of polymers

When either or both of the surfaces are polymers, the contact is often predominantly elastic. Friction of polymers can be attributed to two sources, deformation and adhesion. The friction due to deformation arises from energy dissipation in the bulk of the polymer as the surfaces slide. The friction due to adhesion arises from the asperities on the two surfaces sticking together; a force is needed to break apart these junctions. In most situations both deformation and adhesion will be present.

Polymers deform viscoelastically; the deformation depends not only on the normal load N but also on the geometry and time of loading.

2.1. Friction due to adhesion

At low loads and moderately rough surfaces, the true area of contact is a small fraction of the apparent area, and is proportional to the normal load. The coefficient of friction is therefore constant and independent of the normal load.

At high loads or for very smooth surfaces, the individual asperities merge into one large asperity. For a single elastic asperity the area of contact, A, will be proportional to the load, W, raised to the power $2/3$, this exponent applies to both spherical and cylindrical asperities [2]. The shear strength, τ, of polymers varies with the hydrostatic pressure, σ;

$$\tau = \tau_0 + \alpha\sigma \tag{1}$$

where τ_0 and α are constants for the polymer. But $\sigma = W/A$, $F = \tau A$ and $A \propto W^{2/3}$, therefore the coefficient of friction, $\mu = F/W$, is given by [3];

$$\mu = bW^{-1/3} + \alpha \tag{2}$$

where α and b are constants.

For very high pressures (typically greater than 50 MPa [4]) the real contact area is equal to the apparent contact area. Therefore Eq. (1) leads to:

$$\mu = \frac{\tau}{\sigma} = \frac{\tau_0}{\sigma} + \alpha \tag{3}$$

which tends to α for very high pressures.

2.2. Summation of friction components

Kragelsky et al. [5] support the hypothesis that the coefficient of friction is the sum of two terms; molecular and mechanical, i.e.,

$$\mu = \mu_{\text{molecular}} + \mu_{\text{mechanical}}. \tag{4}$$

Molecular interaction processes take place in the surface 'film' and affect the surface layers to a depth of a few hundredths of a micron. Mechanical interaction takes place in layers with a thickness of a few tenths of a micron. As these processes occur at different levels, they are largely uncorrelated and hence can be separated.

Eq. (4) suggests a very complex relationship between the normal load and the coefficient of friction; both components of μ include a pressure term, as well as extra terms for the hysteresis loss during sliding, the surface roughness, and the strength of the molecular bond, amongst others.

2.3. A modified Howell's equation

With fixed geometry and duration of loading, the area of true contact is proportional to N^{β} where N is the normal load and $(2/3) \leq \beta \leq 1$. For a truly elastic solid (for example rubber), $\beta = 2/3$ [6].

Howell and Mazur [7] performed some of the first experiments to study the effect that the elastic behaviour of the asperity-to-asperity contact has on the nature of sliding for polymeric materials. The stress–strain curves of three hypothetical materials are shown in Fig. 2. The dashed lines represent the stress range in the contacting asperities. The asperities of material (a) deform plastically, so Amon-

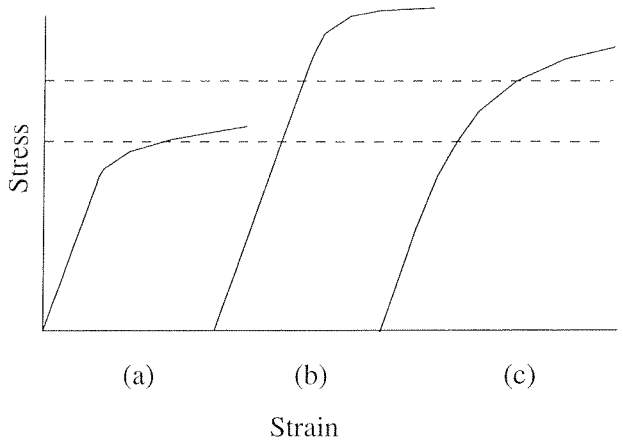

Fig. 2. Stress–strain curves for various hypothetical asperity models; (a) plastic deformation ($F \propto N$), (b) elastic deformation ($F \propto N^{2/3}$), (c) elastic and plastic deformation of asperities ($F \propto N^{\beta}$).

tons' law applies. The asperity-to-asperity contact in material (b) is elastic; so the true asperity-on-asperity contact area will be of the form $CN^{2/3}$ where C involves the modulus and dimensions of the asperities, hence $F = SCN^{2/3}$ (where S is the shear breaking strength). Increasing the normal stress would cause plastic deformations as for material (a).

For material (c) the deformation of the asperity contact starts with a linear elastic region followed by a gradual yield; the true asperity-on-asperity contact area is thus likely to lie between the bounds of materials (a) (plastic $A \propto N$) and (b) (elastic $A \propto N^{2/3}$). Therefore, a possible equation for the friction could be the empirical one, $F = KN^{\beta}$, where $(2/3) \leq \beta \leq 1$. Most synthetic polymers used in ropes correspond most closely to material (c) where the actual mechanism of asperity deformation is indeterminate.

The relationship $F = KN^{\beta}$ fits Howell and Mazur's test results very well; some of their results are shown in Table 1 [7].

Howell's equation for friction can be re-written as $F = (KN^{\beta-1})N$, where $(KN^{\beta-1})$ is the "equivalent coefficient of friction". For use in the finite element analysis it was decided that expressing this relationship in terms of stresses would make modelling possible. Therefore, it is proposed here that Howell's equation be re-expressed by an alternative empirical relationship; $\tau = a\sigma^{\beta}$, where τ is the frictional stress, σ is the contact pressure, and a and β are frictional constants.

2.4. Viscoelastic effects

Due to the viscoelastic properties of polymers, when a polymer is in contact with another surface for a period of time, the asperities start to creep under the normal load. This increases the actual area of contact, thereby increasing the frictional limit. This creep explains why contact involving polymers typically has a greater difference between static and dynamic coefficients of friction than for metal-to-metal contact.

2.5. Yarn-on-yarn friction for Kevlar 49

Briscoe and Motamedi [3] have shown that the yarn-on-yarn coefficient of friction for Kevlar 49 tends to 0.22 for large contact pressures; this is twice as large as the value found here of 0.11 for Kevlar 49 on aluminium. Therefore, there is minimal yarn-on-yarn slip within a Parafil termination, so this parameter is not critical.

2.6. Effect of spin finish on friction

Spin finish is a surface coating, added to the fibres during manufacture for the purpose of gluing together the fibres during the processing of the yarn [8]. This prevents them being snagged by the guides and thus being broken or drawn out of the yarn. The finish also evens out, and so, improves the running properties and friction coefficients, as well as removing any electrostatic charge; these keep the draw-off conditions as even as possible.

Sizes may also be applied to the yarn; these coat the yarn with a protective film to reduce the abrasion damage during processing and service.

By selecting the right finish, the abrasion resistance of the yarn can be increased [9–12]. The yarns used in the tests referred to in this paper are from spools used to make Parafil ropes and so carry the finishes present in actual rope.

3. Kevlar 49 yarn on aluminium capstan friction

3.1. Analysis of yarn-on-capstan friction

The simplest method of measuring the friction between a yarn and a solid is by the capstan method. Here the yarn is pulled over a cylinder of radius R through an angle θ and the end tensions measured (Figs. 3 and 4). Amontons' law leads to (see for example Ref. [13]):

$$T_o = T_i e^{\mu\theta} \tag{5}$$

which is often referred to as the capstan equation and is independent of R. T_i, the incoming tension, is the tension

Table 1
Coefficients and indices of friction, $F = KN^{\beta}$, for various polymers against themselves [7]

Material	K	β
Cellulose acetate	0.60	0.96
Viscose rayon	0.49	0.91
Drawn nylon	0.92	0.80
Undrawn nylon	0.85	0.90

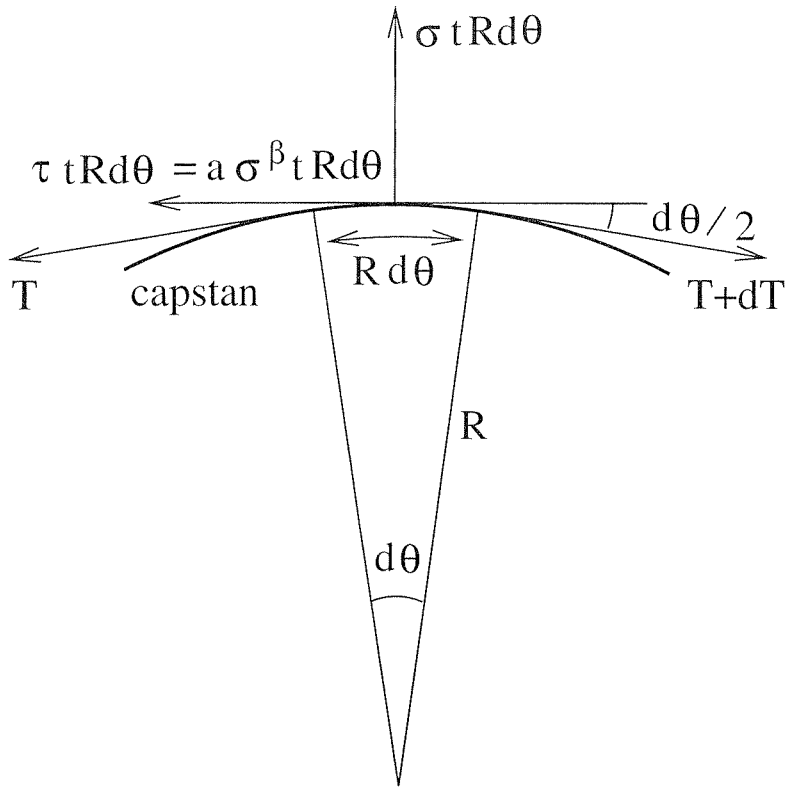

Fig. 3. Forces acting on a segment of yarn running over a capstan.

in the yarn entering the contact zone, between the weights and the capstan. T_o, the outgoing tension, is the tension in the yarn leaving the capstan, between the capstan and the tensometer. μ is the coefficient of friction.

Howell's [14] equation ($F = KN^{\beta}$) leads to:

$$T_o^{1-\beta} = T_i^{1-\beta} + (1-\beta)K\theta R^{1-\beta}. \quad (6)$$

Thus, the radius of the capstan now comes into the equation [15]. If a modified Howell's equation $\tau = a\sigma^{\beta}$ is used, then an alternative equation can be derived. (Note: β is a dimensionless index, but a has dimensions of $(FL^{-2})^{(1-\beta)}$ and thus units.)

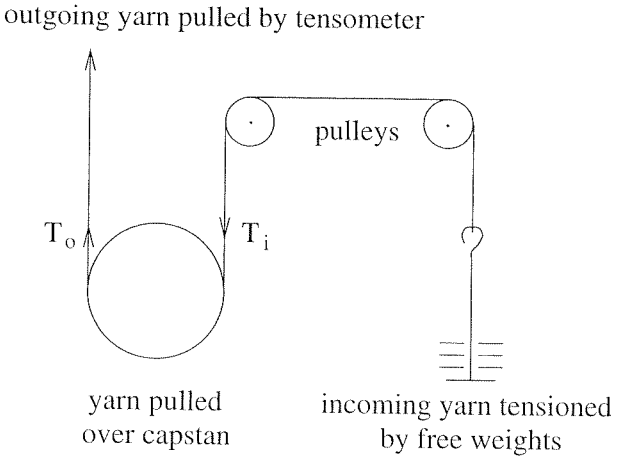

Fig. 4. Apparatus used to measure yarn on solid friction.

Consider a small element of yarn subtending an angle $d\theta$ around a capstan, as shown in Fig. 3. The radius is R, the contact width is t, the contact pressure is σ, and the frictional stress is $\tau = a\sigma^{\beta}$. A resolution of forces along the yarn gives:

$$a\sigma^{\beta} tR\,d\theta = dT. \quad (7)$$

Resolving perpendicular to the contact surface gives:

$$2T\frac{d\theta}{2} = \sigma tR\,d\theta. \quad (8)$$

Eliminating σ from these two equations gives:

$$at^{1-\beta}R^{1-\beta}d\theta = \frac{1}{T^{\beta}}dT. \quad (9)$$

This can be integrated between 0 and θ, and $T = T_i$ to T_o, yielding:

$$T_o^{1-\beta} = T_i^{1-\beta} + (1-\beta)at^{1-\beta}R^{1-\beta}\theta. \quad (10)$$

This equation is then fitted to experimental values of T_o and T_i to give the coefficients a and β that are used in the finite element analysis.

The contact width was taken to be 1.0 mm, both for this analysis, and for the abrasion analysis in Section 5.3. This is consistent with observations of the yarns on the various sized capstans.

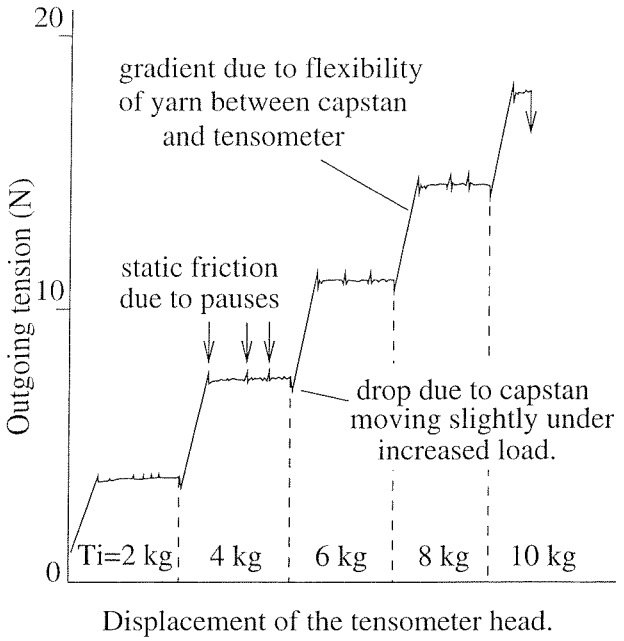

Fig. 5. Plot of the outgoing tension for Kevlar 49 pulled over a 30 mm aluminium capstan at 0.17 mm/s.

3.2. Experimental apparatus

The apparatus consisted of an aluminium capstan over which a Kevlar yarn was pulled, as shown in Fig. 4. The tension in the yarn leaving the contact zone, (the outgoing tension, T_o), was measured by means of the Howden tensometer to which the yarn was tied. The tension in the yarn entering the contact zone, (the incoming tension, T_i), was derived from the free weights applied plus an allowance for the friction in the two pulleys. This allowance was calculated by pulling loaded yarns over two pulleys with no capstan present. For a given incoming tension the tensometer was moved upwards, stretching the yarn between it and the capstan until the force in the yarn was sufficient to overcome friction and the yarn slipped. The use of short lengths of yarn (less than 500 mm connecting the tensometer to the capstan), ensured that little energy was stored, so when slipping occurred it was continuous, and not a series of stick-slip jumps.

For the test shown in Fig. 5 the yarn was stopped to allow it to stick, then re-pulled to see if the new force to initiate sliding was the same as the initial one, which it was.

The yarn was pulled in one direction only to avoid excessive wear of one part of the yarn, and to avoid a build-up of yarn debris.

At the start of a test the apparatus was set up with the lowest free weight in place and the tensometer head raised until slipping took place. More free weights were added, and the procedure repeated until the yarn snapped, usually at the knot attaching it to the tensometer. The test was repeated with a new yarn, ensuring that the earmarked contacting portion was not handled. Between tests the contact area was cleaned with acetone to remove any Kevlar powder that had built up. After many tests it was seen that the aluminium surface had become polished from abrasion. Six tests were each performed on capstans of radii, 10, 20, 30, 40, 50, 60, 70 and 80 mm; each test giving between four and six readings depending on how many loads were applied. A total of 216 readings were taken.

3.3. Experimental equivalent coefficient of friction, μ

Many of the experimental points correspond to low contact stresses, which are not of interest in this analysis. To remove their effect, it is necessary to quantify the contact stresses. A simple analysis for this will suffice, as this is only an indication of the contact stress; Eq. (10) takes into account the variation in contact stress along the length of the contact zone.

A mean contact stress, $\bar{\sigma}$, can be obtained by assuming a uniform contact pressure around the contacting half of the capstan. Resolving forces on the yarn around the capstan, in a direction parallel to the incoming and outgoing yarns, gives:

$$\bar{\sigma} = (T_o + T_i)/2Rt \tag{11}$$

as shown in Fig. 6. To get a mean frictional stress, $\bar{\tau}$, it is assumed that the frictional stress is constant, so looking at the whole contact area gives:

$$\bar{\tau} = (T_o - T_i)/\pi Rt. \tag{12}$$

If Amontons' law applies, then an application of Eq. (5) to the 216 readings of T_o and T_i gives Fig. 7, the contact stress being calculated using Eq. (11). It can be seen that the greater the contact stress the lower the coefficient of friction; this nullifies the assumptions made in deriving this graph, so Amontons' law is not a good model for Kevlar-on-aluminium friction. It is also noted that the coefficient of friction between Kevlar 49 and aluminium is lower than that between Kevlar 49 and itself, which tends to 0.22 at high pressures [3]. This supports the hypothesis that any slip occurring within a Parafil termination does so between the rope and the spike or barrel, rather than within the rope. Therefore, the Kevlar 49 on aluminium abrasion will be the dominant factor in the lifetime of a termination.

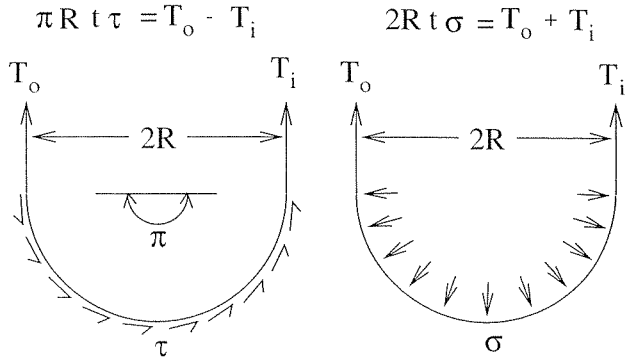

Fig. 6. Estimation of average contact and frictional stresses on a capstan.

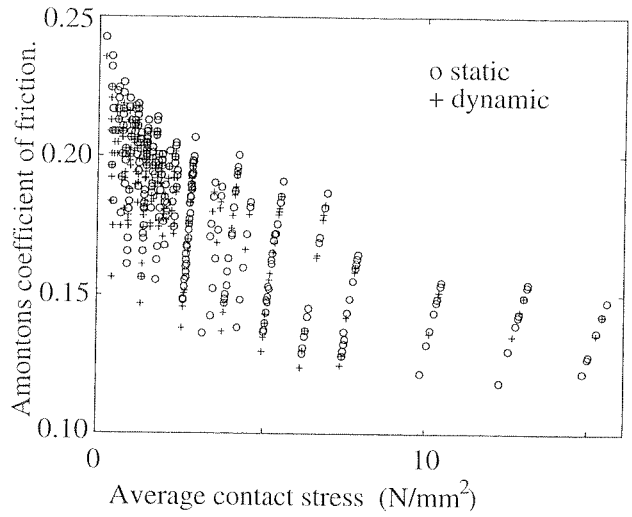

Fig. 7. Effective Amontons' coefficient of friction, μ, for Kevlar 49-on-aluminium assuming μ is constant.

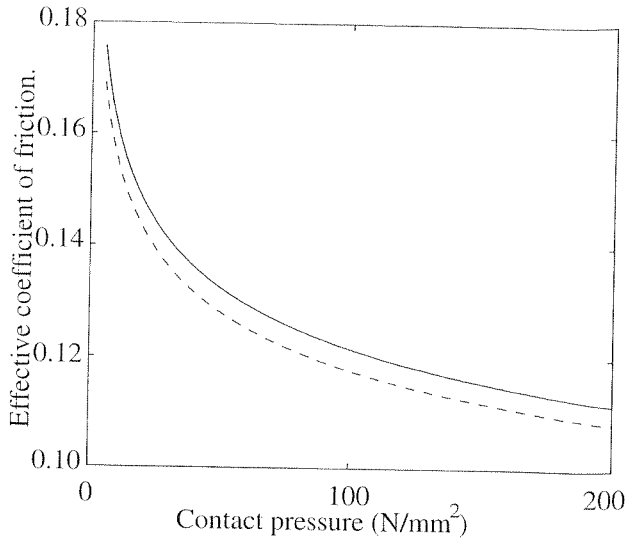

Fig. 9. Equivalent Amontons' coefficients of friction ($\mu = \tau/\sigma$) for Kevlar 49-on-aluminium.

Fig. 8 shows a plot of $\bar{\tau}$ vs. $\bar{\sigma}$. The data points are in pairs; a circle corresponds to a static measurement, and the cross below it corresponds to the accompanying dynamic measurement. It can be seen that the points do not lie on a straight line, and at greater contact pressures the effective coefficient of friction reduces.

3.4. Experimental coefficients of friction, a and β

A best fit equation of the form given in Eq. (10) to all the measured data points (216 static and 216 dynamic) leads to the following two equations:

$$\tau_s = 0.087\sigma^{0.88}, \tag{13}$$

$$\tau_d = 0.084\sigma^{0.88}. \tag{14}$$

However, if an equation of the form given in Eq. (10) is fitted only to the points most relevant to a Parafil termination, which here is taken to be all those with a contact pressure greater than 6 N/mm^2 (21 static and 21 dynamic), then the following refined equations are obtained (where τ and σ are in kN/mm^2):

$$\tau_s = 0.099\sigma^{0.91}, \tag{15}$$

$$\tau_d = 0.095\sigma^{0.91}. \tag{16}$$

These equations are plotted in Fig. 8, the solid line being the static friction and the dashed line the dynamic. Because the static and dynamic indices are the same, these equations give a static friction greater than the dynamic one for all contact stresses. Note, the axes show mean contact and frictional stresses as a way of visualising the experimental data; the actual stresses vary continuously along the length of the contact zone.

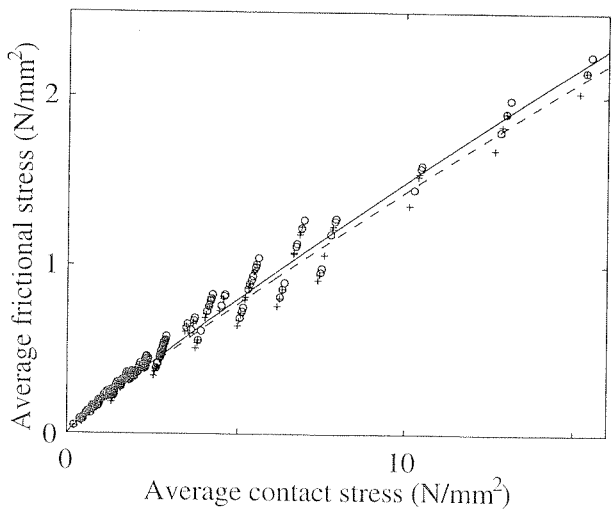

Fig. 8. Visualisation of the average frictional stress vs. average contact stress.

3.4.1. Expressing μ in terms of a and β

Eqs. (15) and (16) can be re-expressed to give equivalent coefficients of friction,

$$\text{static } \mu_s = a_s\sigma^{\beta_s - 1} = 0.099\sigma^{-0.09}, \tag{17}$$

$$\text{dynamic } \mu_d = a_d\sigma^{\beta_d - 1} = 0.095\sigma^{-0.09}. \tag{18}$$

These curves are plotted in Fig. 9 for the range of stress encountered in the finite element analysis.

4. Abrasion of polymeric fibres

Abrasive wear is said to happen when there is a progressive loss of material from the softer surface as two surfaces are rubbed back and forth. In a 'clean' environment this is most often caused by the hard protuberances of one surface gouging grooves in the softer surface as they are reciprocated under normal loading. The swarf is

initially pushed to one side but after many cycles it is removed altogether. If grit is present then this process is speeded up, but Parafil terminations are usually sealed to prevent water penetration, so no grit will be able to get in. Subsurface wear can also accrue from fatigue crack growth in the deformed contact region. In polymers, strong adhesion occurs at the points of contact of the asperities; when sliding occurs, fragments are torn from the softer surface and are left deposited on the harder one [13]. These two classes of wear mechanism, involving subsurface and surface deformation, respectively, are termed cohesive and interfacial wear.

4.1. Archard wear equation

It is possible to form the Archard wear equation either by looking at the contact between asperities, or by looking at the wear caused by many abrasive particles [2]:

$$Q = \frac{KW}{H}. \tag{19}$$

Eq. (19) relates the volume worn per unit sliding distance, Q, to the normal load, W, and the hardness of the softer surface, H. K is the dimensionless wear coefficient.

However, because of the difficulty in defining the plastic hardness H of elastomeric materials, it is often more useful to employ the dimensional wear coefficient, k. k has the units $mm^3(Nm)^{-1}$ and is calculated directly from the volume of material removed by wear per unit distance slid per unit normal load [2]:

$$k = \frac{Q}{W}. \tag{20}$$

5. Kevlar 49 on aluminium abrasion

The shear yield strength of Kevlar 49 is 160 N/mm^2 [16]. Taking the uniaxial yield stress of the aluminium alloy used for the termination to be 600 N/mm^2, then its shear yield strength is 300 N/mm^2 [17]. Therefore, the Kevlar fibres are the softer material and will suffer most of the abrasion.

5.1. Thermal effects

Thermal failure can be avoided (and hence lifetimes improved dramatically) if adequate cooling is provided either by a fan or by water. For Kevlar 29, Du Pont [18,19] have recorded only small reductions in the tensile strength (about 20%) up to 180°C followed by large reductions above this; Kevlar 49 is similar.

Even at the very high stresses, 5%–70%, and frequencies, 0.33 Hz, to which Crawford and McTernan [10] subjected a 150 tonne Parafil F (Kevlar 29) rope, the temperature did not rise above 100°C due to Kevlar's low hysteresis and the absence of lay geometry. Thermocouples were inserted into the rope core at the front face of the termination. Thermal failure would not be expected to occur at this temperature, and the ropes failed by mechanical abrasion. They reported only split fibres, which would be expected in a fretting failure at low amplitudes of motion.

5.2. Creep rupture effects

At high stresses, creep-rupture may be a significant factor. Kenney et al. [20] have carried out many tests on nylon fibres, yarns and small ropes, subjecting them to cyclic axial stress. They found that yarns and single fibres fail by creep-rupture (i.e., they creep to failure), which depends on the total time that the loads are applied rather than the number of cycles. They also showed that the behaviour of other oriented fibres including polyester and aramid (e.g., Kevlar) agrees with this cumulative-time-under-load model.

Lyons et al. (reported in Ref. [21]) have shown that there are two distinct regions in the strain–cycles-to-failure curve, with extremely long lives occurring for low strains. Kenney et al. cycled across these two regions, thus masking this phenomenon.

Crawford and McTernan [10] performed low-load cyclic tests at different frequencies, thus subjecting the ropes to different times under load for a given number of cycles. They found that the frequency had no discernible effect on the number of cycles to failure. Cyclic loading at high stresses is not envisaged for Parafil, so creep-rupture has not been a part of this study.

5.3. Abrasion of Kevlar 49 yarns on aluminium capstans

A comprehensive study of abrasion of Kevlar 49 yarn on aluminium has been undertaken. There are many variables that may affect the lifetime of a yarn rubbing on a solid; the amplitude of the cycle, the contact pressure, the maximum load and hence the amount of yarn to be abraded, the surface finishes of the materials including the 'size' that is applied to the yarn, the temperature, the presence of debris and the presence of water. For this analysis it has been assumed that only the amplitude, the contact pressure and the thickness to be abraded are significant variables.

Actual rope yarns were used, with no alteration made to their surface coatings; the materials were kept as clean and dry as possible, and all tests were performed at room temperature (although the temperature in a rope under cyclic loading may rise to 100°C).

For this analysis it is assumed that the rate of wear is uniform throughout a test. This is a reasonable assumption as the Kevlar debris is removed from the aluminium

surface by the rubbing of both the yarns in these tests and the yarns in the rope terminations, thus ensuring fresh material is always in contact. Also, the Kevlar away from the contact zone moves as one and does not abrade against itself, so whilst it is away from the aluminium surface it is unaffected by the number of cycles accrued.

5.4. Experimental yarn on capstan apparatus

Fig. 10 shows a schematic view of the abrasion tester that was built to perform lifetime tests.

A yarn was passed over a disc of the desired radius, to make the desired contact angle. For small angles of contact the exact value is not relevant in determining the contact pressure, however, the contact zone should be long enough such that a portion of yarn is subjected to the entire regime. If a piece of yarn passed outside the contact zone at both ends of the cycle, then no part of the yarn would be fully abraded. The contact length must also be short enough that the tension in the yarn does not rise too much, due to friction, to affect the contact pressure. A contact angle of 10° was used throughout.

Considering a small element of yarn passing over the disc and resolving normal to the surface, $\sigma R\theta t = 2T\theta/2$, or $\sigma = R/Tt$. R is the radius of curvature, T is the yarn tension, σ is the contact stress, and t is the width of the contact zone, which was taken to be 1 mm.

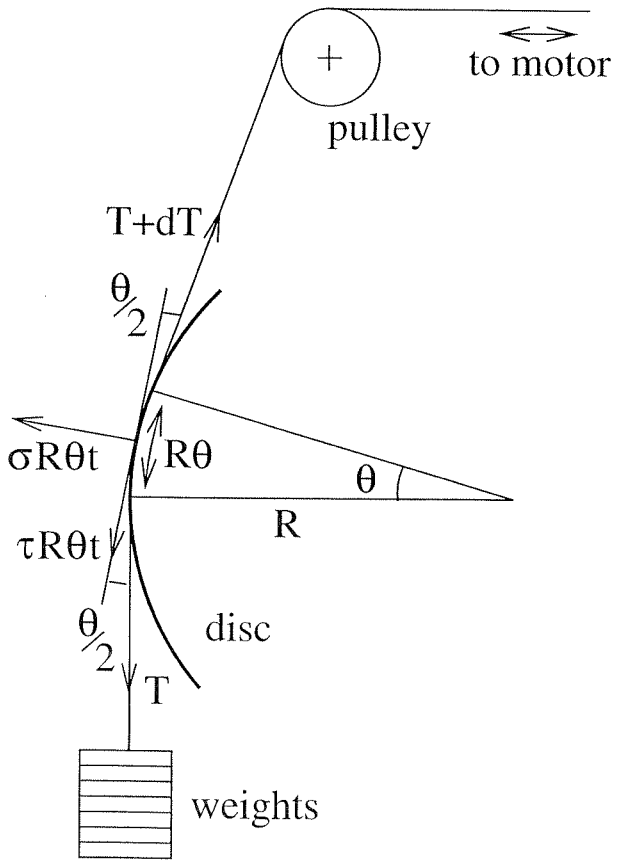

Fig. 10. Schematic of apparatus used to determine yarn-on-solid abrasion.

The yarn was guided over the disc by means of pulleys. One end was driven by a motor via an eccentric axle, which gave rise to a sinusoidal oscillation. The movement was constrained with bearings to translate this rotation into a linear motion. The other end was loaded by a free weight. To stop the free weight spinning and hence removing all the twist present in the yarn, it was loosely tied to a cut-off switch with a piece of thick wire. The weight would rotate round by a quarter of a turn until the wire exerted enough torque to prevent the yarn untwisting further; the wire was set such that it provided no axial load into the system. When the yarn broke, this piece of wire would pull a block out of a cut-off switch, thus stopping both the motor and the counter.

A marker was attached to the yarn just above the weight, and the upper and lower limits of this marker noted by a travelling microscope; the position was read from the Vernier scale on the side of the microscope. These readings were repeated six times and a mean taken to give the amplitude of each cycle.

All the abrasion tests were performed using Kevlar 49 yarn from a bobbin used to make Parafil ropes provided by Linear Composites. Therefore, the number of fibres present, the amount of twist and the size applied to the yarns are all representative of those within a Parafil termination. When assembling the apparatus care was taken to ensure that the number of twists in the yarn remained constant (about 45 turns per metre). The aluminium discs were prepared by sawing a template out of Dural, then turning this in a lathe.

The surface of an aluminium 60 tonne Parafil G spike has small shallow grooves running around it every 0.25 mm. It was not practical to machine these on the discs used here, as they are a by-product of the turning process in manufacturing the spike. Experiments were done with score marks running perpendicular to the direction of slip, but it was not possible to create the smooth score marks that are found on the spike, and so the lifetimes were exceedingly short.

The discs here were smoothed as much as possible for the first test, and after several abrasion tests were performed it could be seen that the already smooth surface was polished even more by the abrasion from the Kevlar. A fine yellow dust was present around the contact zone from the debris.

The yarn was clamped at both ends between aluminium plates that are screwed together; this is a very efficient method of restraining the ends, as this restraint remains effective regardless of the number of fibres that have broken. It was found to be impractical to glue the ends as it was very difficult to achieve a uniform coating on all the fibres whilst maintaining their geometry within the yarn. A frequency of 2 Hz was chosen, this being the highest speed possible before dynamic effects from the flexibility of the

rig became significant. The change in tension due to the dynamic loading on the free weight was negligible at this speed.

For the fixed amplitude experiments the peak to peak amplitude was fixed at 0.68 mm and the contact pressure and thickness to be abraded were altered by using discs of radii 27.5 and 79.5 mm, with loads of 50.0, 100.2, 150.0 and 199.8 N. Other experiments were done using peak to peak amplitudes of 0.12, 0.68 and 2.90 mm, corresponding to very small maximum sliding speeds of 0.75, 4.27 and 18.2 mm/s ($=2\pi\ f(a_0/2)$).

5.5. Calculation of wear rate for yarn on capstan abrasion

For this analysis it is assumed that under a certain severity, determined by the contact pressure and the amplitude, the rate of wear of the Kevlar 49 is constant. This is not necessarily true; the rate may slow down due to a build-up of debris which will act as a lubricant and as a barrier, and conversely the rate may speed up due to damage being accumulated above the contact zone from inter-fibre fretting.

The cross-sectional area of the yarn is taken to be 0.23 mm^2. This area correlates with the breaking load of 440 N (taken from a mean of six tensile tests using Amani-ampong's jaws [22]) and the rope's ultimate tensile stress of 1926 N/mm^2. It is assumed that the yarn deforms over the capstan into a rectangle 1 mm wide and 0.23 mm thick, which is consistent with observations for all the severities measured.

For the yarn experiments, the thickness that needs to be abraded before failure occurs is related to the maximum tension in the yarn. For a larger tension less material needs to be abraded before the remaining yarn reaches its breaking stress. The proportion of yarn that has abraded at failure is $(1-\lambda_{max}/100)$ where λ_{max} is the percentage ratio of the maximum load to the breaking load, therefore the thickness that has been abraded, δ, is $0.23\times(1-\lambda_{max}/100)$.

The wear rate is calculated from this thickness as follows:

$$\text{volume abraded} = r\theta\delta t, \tag{21}$$

$$\text{normal load} = T\theta, \tag{22}$$

$$\text{distance slid} = 2a_0N, \tag{23}$$

where r is the radius of the capstan, θ is the angle of contact zone subtended, t is the width of the contact zone, T is the tension in the yarn, a_0 is the peak to peak amplitude of cycling and N is the number of cycles to failure. Therefore:

$$k = \frac{\text{volume abraded/distance slid}}{\text{normal load}},$$

$$k = \frac{r\delta t}{2a_0NT}. \tag{24}$$

5.6. Lifetimes of Parafil terminations

Very little data has been published for the abrasion lifetimes of Parafil ropes. Some data has been obtained from tests performed at the National Engineering Laboratory on Parafil G ropes. These include tests on 6 tonne ropes with cyclic ranges of 5%–35%, 10%–50%, 25%–55%, 20%–60%, 10%–70% [23], 15%–45%, 5%–55% [24], and 15%–65% [25]; and 60 tonne ropes cycled between 5%–30%, 5%–35%, 5%–40%, 5%–50%, 5%–70% [26]. (An x% load refers to x% of the nominal breaking load of the rope.)

There is no overall scheme to this data, since different maximum and minimum load limits were used throughout. The data for these 6 and 60 tonne Parafil G ropes is plotted in Fig. 11; the y-axis is taken to be the maximum load. (The ranges do not form smooth zones because the minima are different.) It is clear that the 60 tonne ropes have a much shorter lifetime than the 6 tonne ropes. This is due to the larger amplitude of abrasion that is occurring within them.

For the 6 tonne rope, the greatest lifetimes are achieved by the regimes having a 30% cycle ($\lambda=5$ to 35, 15 to 45 then 25 to 55 (where λ is the percentage ratio of load to maximum static strength)); next come the regimes with 40% cycles ($\lambda=10$ to 50 then 20 to 60) followed by 50% ($\lambda=5$ to 55 and 15 to 65) then finally the 10% to 70% cycle. This indicates that it is the amplitude of the cycle, both in terms of load and therefore slip, that is more significant than the maximum load. All the 25% to 55% tests outlived all the 10% to 50% tests, due to their smaller amplitude, despite having a greater maximum load. They also outlived the 5% to 55% tests by an order of magnitude.

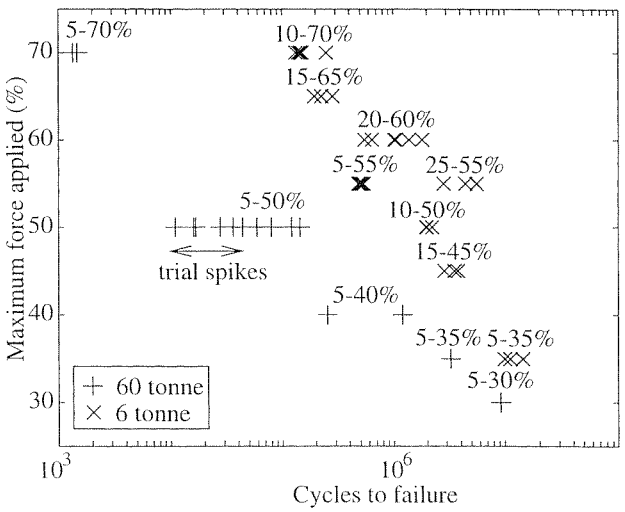

Fig. 11. The lifetimes of 6 and 60 tonne Parafil G ropes subjected to cyclic loading.

5.7. Calculation of wear rate in Parafil terminations

Using the results from a finite element analysis [1], it is possible to predict a maximum yarn-on-spike amplitude of movement and associated contact pressure for each of these rope tests. The contact pressure is determined from the maximum preload that has been applied.

A Parafil rope is terminated by removing a length of sheath equal to the length of spike, and evenly distributing the yarns around the circumference of the barrel. The spike is guided home as the rope is drawn through the barrel. For this the barrel is supported vertically, and the sheath of the rope pulled down by hand. For the final assembly the spike is tapped with a hammer while pulling the rope.

When a Parafil rope is loaded for the first time, the spike is pulled further into the barrel by the rope; it "beds-down". This preloading generates a transverse contact pressure between the rope and spike and the rope and barrel, this pressure locks the spike into the termination.

It is not known what each maximum preload was for the literature data, so for this analysis it is assumed that the maximum load in the cycle is also the limit of the preload. It is assumed that the contact stresses in the termination are solely determined by the maximum load applied, and

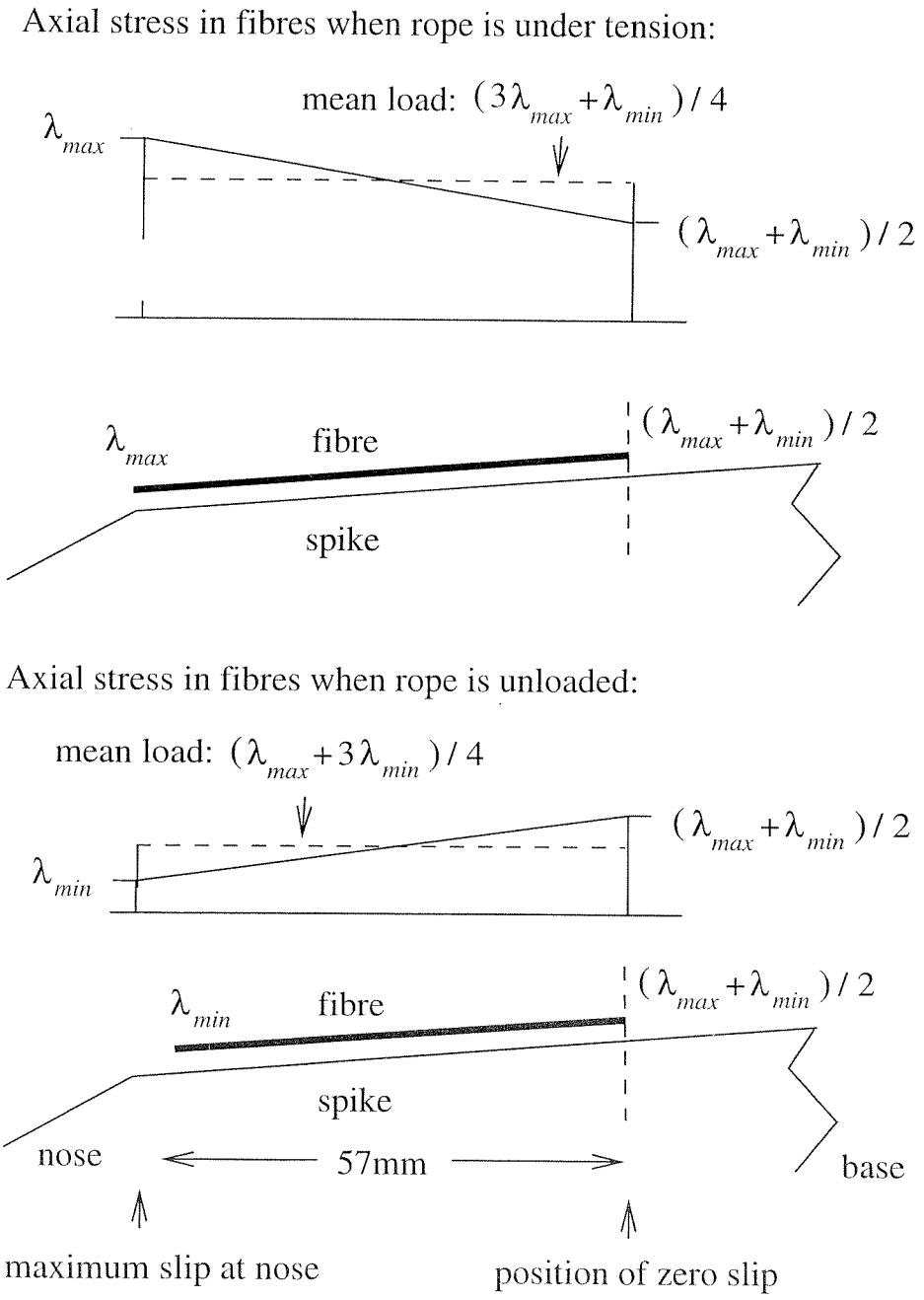

Fig. 12. Schematic of the idealised load variation within a termination.

are not size dependent; i.e., a 6 tonne rope at 50% load will have the same contact pressure between the rope and spike as a 60 tonne rope at 50% load. This follows from the scaling used to design the terminations. The contact pressure–preload relationship can be linearised [1] to give:

$$\sigma = 1.30 \times \lambda_{max} \tag{25}$$

where λ_{max} is the maximum percentage load factor applied (100 × maximum load/breaking load), and σ is the contact pressure between the spike and rope, and between the rope and barrel in N/mm^2.

To estimate the amplitude of slip it is found from the finite element analysis that there is a position on the spike where no relative slip occurs. If it is assumed that this is the case for all rope sizes, and for all the regimes, then the slip can be quickly estimated by analysing the portion of rope between this location and the nose of the spike. Fig. 12 shows a schematic diagram of the forces that are present in the fibres at the load cycle limits for a 60 tonne Parafil G rope. From the finite element analysis it is noted that the rope remains static at 163 mm from the base of the spike and rubs over the nose at 220 mm from the base, so 57 mm of rope is stretched within the termination.

At the non-moving location, the axial stress in the rope is assumed to remain constant irrespective of the force in the rope. At the nose of the spike the load in the rope varies between λ_{max} and λ_{min}. The friction is taken to be uniform along the length of the slipping region. Therefore, the tension in the fibres will vary linearly along their length. Hence, the load at the non-moving point will be the mean of λ_{max} and λ_{min}, as seen in Fig. 12 (assuming an equal friction applies in both directions).

The extension in the fibres can be calculated by integrating the strain along the stretched portion. Due to the assumed linearity, the mean load in the rope can be used to calculate the extension. The maximum load case is equivalent to a uniform load of $(3\lambda_{max} + \lambda_{min})/4$, and the minimum to $(\lambda_{max} + 3\lambda_{min})/4$. The difference between these gives the magnitude, λ_0, for an equivalent uniform cyclic loading of $(\lambda_{max} - \lambda_{min})/2$.

The total cyclic strain, ϵ_0, can be expressed as a fraction of the longitudinal failure strain, ϵ_y, thus:

$$\epsilon_0 = \frac{\lambda_0}{100}\epsilon_y = \frac{\lambda_{max} - \lambda_{min}}{2 \times 100}\epsilon_y \tag{26}$$

Multiplying ϵ_0 by the length of the stretched region, 57 mm, and substituting in the value of $\epsilon_y = 0.015$ for Kevlar 49 [27], gives the amplitude of slip, a_0;

$$a_0 = 57\epsilon_0 = 4.28 \times 10^{-3}(\lambda_{max} - \lambda_{min}). \tag{27}$$

For a 5%–50% cycle in a 60 tonne rope this gives a displacement of 0.19 mm compared with the finite element result of 0.20 mm.

It is assumed that the areas of different sized terminations are scaled linearly, such that the cross-sectional area of a rope of size, Q tonne, will be related to a 60 tonne rope by the factor $Q/60$. Therefore the lengths will be scaled by a factor of $\sqrt{Q/60}$.

Hence, the amplitude of slip becomes:

$$a_0 = 4.28 \times 10^{-3}(\lambda_{max} - \lambda_{min})\sqrt{Q/60}. \tag{28}$$

The compressed thickness of the rope at the nose of a 60 tonne Parafil G rope is 3.2 mm from the finite element analysis (which is an annulus of 320 mm^2 at a mean radius of 16 mm). The thickness to be abraded, δ, that needs to fail from each side of the rope, for the failure stress to be reached in the remaining rope at the maximum load, is given (for a rope of size Q tonne) by:

$$\delta = 3.2 \times \frac{100 - \lambda_{max}}{100} \times \frac{1}{2} \times \sqrt{\frac{Q}{60}}. \tag{29}$$

It is assumed that an equal amount of wear takes place between the rope and spike and the rope and barrel. Therefore the wear rate is calculated by looking at the contact between the rope and the spike only. The wear rate is calculated from this thickness as follows:

$$\text{volume abraded} = l2\pi r\delta, \tag{30}$$

$$\text{normal load} = 2\pi rl\sigma, \tag{31}$$

$$\text{distance slid} = 2a_0 N, \tag{32}$$

where r is the radius of the spike ($= 16.0 \times \sqrt{Q/60}$), l is the length of contact zone, a_0 is the peak to peak amplitude of cycling and N is the number of cycles to failure. Therefore:

$$k = \frac{\text{volume abraded/distance slid}}{\text{normal load}},$$

$$k = \frac{\delta}{2\sigma a_0 N}. \tag{33}$$

5.8. Results of wear rate vs. load

Fig. 13 shows the average wear rate for each test against the normal load. There are three distinct groups

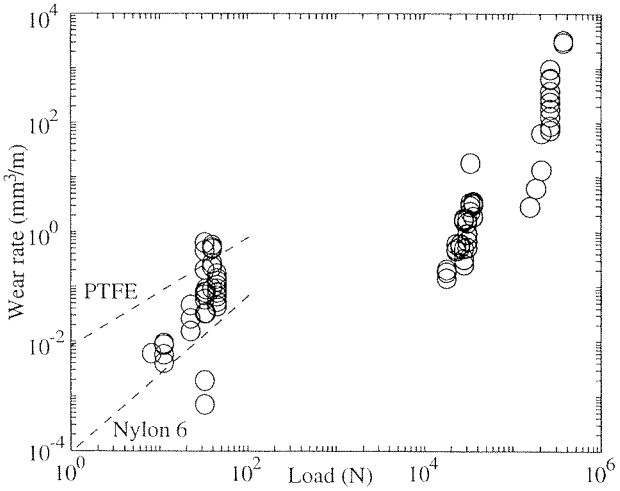

Fig. 13. Effect of normal load on wear rate.

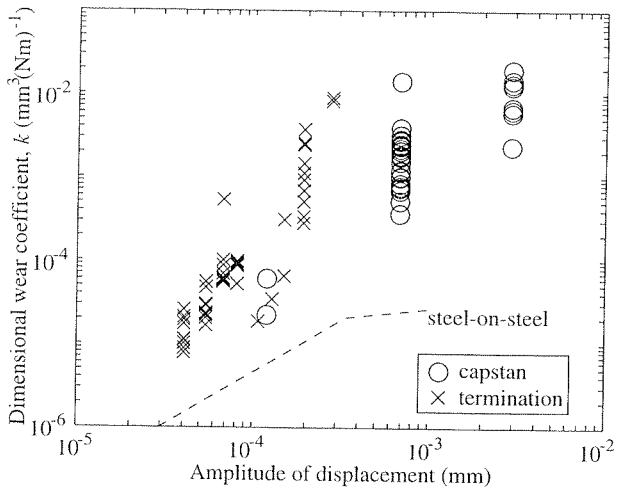

Fig. 14. Effect of amplitude on dimensional wear coefficient.

present, these are due to the vastly different normal loads present in the capstan, 6 and 60 tonne rope experiments. The three groups lie on a line whose gradient is similar to those found for PTFE and Nylon 6 sliding against a mild steel counterface [28], these being represented by the dashed lines.

From this it can be seen that the wear rate increases with normal reaction. Archard's equation implies that the wear rate should be directly proportional to the normal load, i.e., a log–log graph should have a gradient of unity. The gradient here is slightly less than this, although it is considered close enough for the use of Archard's equation.

5.9. Results of dimensional wear coefficient vs. amplitude

For metals the wear rates depend on the amplitude of the sliding. At amplitudes less than 1 μm the two surfaces are stuck and negligible wear takes place. Up to 10 μm, microslip starts occurring with a rise in wear rate. Between 10 and 300 μm, gross slip occurs and there is a large rise in k. Beyond this level reciprocating sliding is occurring and the value of k has generally plateaued. For comparison with Kevlar, steel on steel wear is shown on Fig. 14 [29].

The relationship between the dimensional wear coefficient, k, of Kevlar 49 on aluminium and the peak to peak amplitude of reciprocal motion is shown in Fig. 14. There is no plateau evident — there is a uniform rise in the dimensional wear coefficient with amplitude, the values being typically one to two orders of magnitude greater than for steel-on-steel for the range of displacements measured.

5.10. Ratner–Lancaster correlation

The product of the ultimate tensile stress and elongation for the polymer, σ_u and ϵ_u, is roughly proportional to the area under the stress–strain curve to the point of tensile rupture, and so provides a measure of the work done in producing tensile rupture. Despite the conditions of measurement of these quantities varying from the conditions under which abrasion takes place, it is found for many polymers that there is a good agreement between $1/\sigma_u\epsilon_u$ and k [30].

The longitudinal properties of Kevlar 49 are $\sigma_u = 1926$ N/mm^2 and $\epsilon_u = 0.015$ [27]. This leads to an estimated k of 2.0×10^{-3} mm^3(Nm)$^{-1}$ [30], which lies in the middle of the values of k observed.

6. Conclusions

(1) With the appropriate experiments it is possible to gather the friction data that is required for a finite element analysis of a Parafil termination. For Kevlar 49-on-aluminium this takes the form $\tau_s = 0.099\sigma^{0.91}$ and $\tau_d = 0.095\sigma^{0.91}$.

(2) Kevlar 49-on-Kevlar 49 friction is not critical in the mechanics of the terminations.

(3) In a similar way, Kevlar 49-on-Kevlar 49 abrasion is not critical in the lifetimes of terminations.

(4) The wear rate is directly proportional to the normal load so Kevlar 49-on-aluminium abrasion can be expressed in terms of the Archard wear equation.

(5) The dimensional wear coefficient depends strongly on the amplitude of slip, rising from 1.0×10^{-5} mm^3(Nm)$^{-1}$ at 40 μm to 1.0×10^{-2} mm^3(Nm)$^{-1}$ at 3 mm peak to peak displacement.

(6) This work, which focused on understanding behaviour, can therefore be extended to optimise the design of Parafil terminations in terms of materials and geometry for bigger and longer lasting ropes.

Acknowledgements

The authors would like to thank Linear Composites for permission to use the Parafil rope test data. One of the authors (Brown) was partly funded by the Science and Engineering Research Council and by Fitzroy Systems.

References

[1] I.F. Brown, Abrasion and Friction in Parallel-lay Rope Terminations, PhD Thesis, CUED, 1997.
[2] I.M. Hutchings, Tribology, Friction and Wear of Engineering Materials, Edward Arnold, London, 1992.
[3] B.J. Briscoe, F. Motamedi, The ballistic impact characteristics of aramid fibres: the influence of interface friction, Wear 158 (1992).
[4] F. Van De Velde, P. De Baets, The friction and wear behaviour of polyamide 6 sliding against steel at low velocity under very high contact pressures, Wear 209 (1997).

[5] I.V. Kragelsky, M.N. Dobychin, V.S. Kombalov, Friction and Wear, Calculation Methods, Pergamon, Oxford, 1982.
[6] B. Lincoln, Frictional and elastic properties of high polymeric materials, British Journal of Applied Physics 3 (1952) .
[7] H.G. Howell, J. Mazur, Amontons' law and fibre friction, Journal of the Textile Institute 44 (2) (1953) .
[8] B. Piller, Bulked Yarns, Textile Trade Press, Manchester. 1973.
[9] D.E. Beers, J.E. Ramirez, Vectran fiber for ropes and cables, Marine Technology Society '90 Proceedings, Washington, 1990.
[10] H. Crawford, C.M. McTernan, 'Fatigue' properties of Parafil, Symposium on Engineering Applications of Parafil Ropes, London, 1988.
[11] M.J. Schick, Surface Characteristics of Fibres and Textiles: Part I, Marcel Dekker, New York, 1975.
[12] M.J. Schick, Surface Characteristics of Fibres and Textiles: Part II, Marcel Dekker, New York, 1977.
[13] R. Meredith, J.W.S. Hearle, Physical Methods of Investigating Textiles, Textile Book Publishers, New York, 1959.
[14] H.G. Howell, The general case of friction of a string round a cylinder, Journal of the Textile Institute 44 (8/9) (1953) .
[15] D.G. Lyne, The dynamic friction between cellulose acetate yarn and a cylindrical metal surface, Journal of the Textile Institute 46 (1) (1955) .
[16] S. Kawabata, M. Sera, Torsional fatigue of aramid fibers, Proceedings of the International Conference on Advanced Composites, Wollongong University, Australia, 1993.
[17] M.F. Ashby, D.R.H. Jones, Engineering Materials 1, Pergamon, 1980.
[18] Du Pont, Characteristics and uses of Kevlar 29 aramid, Bulletin No. 375, E.I. Du Pont de Nemours and Co., Wilmington, 1976.
[19] Du Pont, Kevlar para-aramid; database for fibre optic and other cables, E.I. Du Pont de Nemours and Co., Wilmington, 1988.
[20] M.C. Kenney, J.F. Mandell, F.J. McGarry, Fatigue behaviour of synthetic fibres, yarns, and ropes, Journal of Material Science 20 (1985) 2045–2059.
[21] J.W.S. Hearle, Fatigue in fibres and plastics (a review), Journal of Material Science 2 (1967) 474–488.
[22] G. Amaniampong, Variability and viscoelasticity of parallel-lay ropes, PhD Thesis, CUE, 1992.
[23] Technomare, Personal communication, 1996.
[24] L.M. McTernan, Personal communication, 1986.
[25] L.M. McTernan, Comparative tests on 6 tonne Type G Parafil cables and terminations, National Engineering Laboratory, personal communication, 1992.
[26] L.M. McTernan, Second Interim Report on Testing of 60 tonne Parafil Type G (Kevlar 49) Rope and Terminations, National Engineering Laboratory, 1986.
[27] Linear Composites, Parafil Rope Technical Note 1, Linear Composites, Vale Mills, Oakworth, W. Yorkshire, 1977.
[28] D.C. Evans, J.K. Lancaster, in: D. Scott (Ed.), Wear, Treatise on Materials Science and Technology, Academic Press, Vol. 13, 1979, pp. 85–139.
[29] O. Vingsbo, S. Söderberg, in: K.C. Ludema (Ed.), Wear of Materials, ASME, 1987, pp. 885–894.
[30] B.J. Briscoe, Wear of polymers: an essay on fundamental aspects, Tribology International 14 (1981) 231–243.